Applied Thermal Engineering 231 (2023) 120891

Contents lists available at ScienceDirect

Applied Thermal Engineering

journal homepage: www.elsevier.com/locate/apthermeng

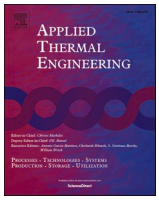

Research Paper

An analytical solution for heat and mass transfer in falling film absorption with arbitrary thermal boundary conditions

Mahyar Ashouri, Amin M. Elsafi, Ilya S. Girnik, Majid Bahrami *

Laboratory for Alternative Energy Conversion (LAEC), the School of Mechatronic Systems Engineering, Simon Fraser University, Surrey, BC, Canada, and Pacific Institute for Climate Solutions (PICS), Canada

ARTICLE INFO

Keywords:
Absorption system
Analytical solution
Falling film
Heat and mass transfer
Non-volatile absorbents
the Laplace transform

ABSTRACT

Absorption, the process of capturing the absorptive component in the volume of the absorbent, is essential for various industrial applications. Several analytical solutions exist for falling film absorbers, which is the most common absorber used in industrial applications. However, in existing models, the temperature of the heat transfer fluid has been assumed to be constant, while the design of falling film absorbers for absorption heat pumps requires an analytical model accounting for the variation in the heat transfer fluid temperature changes. This study presents a new and comprehensive analytical solution for non-volatile absorbents using the Laplace transform method, where an arbitrary heat flux is applied to the heat exchanger wall in contact with the heat transfer fluid. For the first time, this study provides analytical solutions for various wall boundary conditions, including arbitrary heat flux, isothermal, as well as mean, linear, and exponential temperature variation of the heat transfer fluid. The present model is validated with experimental data available in the literature with a relative difference of 11% for several absorber configurations. Considering a case study of an absorber with a length of 1 m, it is shown that assuming an average temperature for the heat transfer fluid overestimates the optimal length of the absorber and results in up to 3 times the absorption rate at the outlet region of the absorber compared to a linear and an exponential temperature estimation.

1. Introduction

Fossil fuels are the primary energy source for heating and cooling in residential buildings and are considered to be one of the main contributors for climate change [1,2]. About 40% of the total energy usage in developed countries is used for space heating, cooling, and domestic hot water production [3,4]. Most jurisdictions in North America and other developed countries have set ambitious goals to increase the installation of electric heat pumps in order to reduce the greenhouse gas emissions produced by buildings. However, the radical and complete replacement of fossil fuels with renewable electricity for heating may not be feasible and could lead to significant 'capacity wastes':

i) Renewable generation capacity waste due to the significant variation of the total energy demand between summer and winter. This issue is much more profound in colder climates. Based on a recent study in the UK, it is estimated that an additional three times the current renewable electricity capacity is required for the heating demand in winter, assuming that the average seasonal Coefficient of Performance (COP) of the heat pump is 2.5–3 and the daily energy storage is already in place, which will be mostly idle in other seasons [5];
ii) The existing electrical grids cannot handle the all-electric heating demand, particularly, in densely populated areas, in addition to the fast-increasing load from the electrification of the transport sector. It requires a tremendous increase in grid size – which would be extremely costly – and takes years for the distribution infrastructure and grid upgrades; and
iii) The existing vapor compression heat pumps run on electricity, which although, this is not the case in British Columbia, globally it is predominantly produced from fossil fuels. Approximately 76% of global electricity is generated by burning fossil fuels [6].

Therefore, there is an urgent need to develop alternative heating, cooling, and thermal energy storage technologies to achieve decarbonization and to meet the Clean BC Roadmap to 2030 [7] and Paris Agreement [8] targets.

Absorption heat transformation systems are a promising alternative to electrical heat pumps for domestic heating and cooling applications.

* Corresponding author.
E-mail address: mbahrami@sfu.ca (M. Bahrami).

https://doi.org/10.1016/j.applthermaleng.2023.120891
Received 27 February 2023; Received in revised form 2 June 2023; Accepted 4 June 2023
Available online 9 June 2023

Nomenclature

Bi	Biot number
c	Concentration of absorbate, $kg.kg^{-1}$
c_s	Isobaric specific heat, $J{\cdot}kg^{-1}K^{-1}$
D_s	Mass diffusivity, $m^2{\cdot}s^{-1}$
g	Gravity, $m{\cdot}s^{-2}$
h_{abs}	Heat of absorption, $kJ.kg^{-1}$
Le	Lewis number, $[Le = \alpha.D^{-1}]$
L	Length, m
L_c	Characteristic length, m
N_{tube}	Number of tubes
$\dot{m}$	Absorption rate, $kg{\cdot}m^{-2}s^{-1}$
$\dot{q}$	Heat flux, $W{\cdot}m^{-2}$
$\dot{Q}$	Dimensionless heat flux
T	Temperature, K
u	Streamwise velocity, $m{\cdot}s^{-1}$
v	Normal velocity, $m{\cdot}s^{-1}$
x	Local tangential position, m
y	Local normal position, m

Greek symbols

α	Thermal diffusivity, $m^2{\cdot}s^{-1}$
φ	Angle
γ	Dimensionless mass fraction distribution
η	Dimensionless normal position
$\boldsymbol{\xi}$	Dimensionless streamwise position
Λ	Normalized heat of absorption
θ	Dimensionless temperature distribution
μ	Mass transfer potential
Γ	Solution mass flow rate per unit depth $kg{\cdot}s^{-1}m^{-1}$
δ	Film thickness, m
ρ	Density, $kg{\cdot}m^{-3}$
ν	Kinematic viscosity, $m^2{\cdot}s^{-1}$

Subscripts

eq	Equilibrium
HTF	Heat transfer fluid
inf	Interface
l	Local
o	Entrance region
s	Solution
t	Total
w	Wall

These systems may also be used for thermal storage, CO_2 capture, and dehumidification [9–11]. Their main advantage over vapor compression systems is that they can be designed to be driven by low-grade waste heat that can be supplied from thermal solar panels, geothermal sources, industrial waste heat, or other sources [12]. However, there are still challenges with the existing absorption systems, including: i) corrosion [13]; ii) crystallization [14]; and iii) poor performance, as well as maintenance issues and most importantly, the cost [15]. The literature proposes methods to overcome some of these challenges, such as coating heat exchangers to prevent corrosion [14] and implementing proper control strategies to prevent crystallization [16].

Developing high-performance absorbers is the cornerstone of designing a competitive and efficient absorption heat transformation system. Heat and mass transfer simultaneously occur in absorbers, therefore, developing an in-depth understanding of the pertinent heat and mass transfer processes in absorption sorber beds is critical.

Several numerical studies exist for the most common absorber designs in the literature, i.e., the falling film absorbers [17]. However, implementing numerical methods requires high computational time and their results are restricted to a specific geometry or design with the selected operating conditions, therefore, reducing their usability. A generalized analytical solution can resolve these issues and makes design, optimization, real-time control, and parametric studies possible in a timely manner.

Three different analytical methods are available in the literature to calculate the coupled heat and mass transfer in laminar falling film absorption. These models are based on: i) the similarity solution [18,19]; ii) the Fourier method [20]; and iii) the Laplace transform method [21,22]. More detailed information for the mentioned studies can be found in our previous study [15]. As shown in Table 1, previous studies have focused on either isothermal or adiabatic boundary conditions for falling films.

In a recent study, we [15] compared the abovementioned solution methods and concluded that:

i) The similarity solution method may not result in accurate results, especially at the film entrance region, where there is no similarity between the temperature profiles;
ii) Although, analytical solutions obtained by the Fourier method provide reasonable accuracy, except for at the entrance region, the eigenvalues should be numerically calculated for each operating condition. This requires computation that makes the solution difficult to use under operating conditions in real systems; and
iii) The Laplace transform method can result in a solution with reasonable accuracy provided that a suitable velocity profile is used.

Based on the above literature summarized in Table 1, the temperature of the heat transfer fluid has been assumed to be constant in all previous analytical studies, while the design of falling film absorbers for absorption heat pumps requires an analytical model accounting for the variation in the heat transfer fluid temperature. Therefore, this study aims to develop a new analytical solution that accounts for the effect of variation in the heat transfer fluid temperature on the heat and mass transfer in falling film absorbers. The model is developed based on the Laplace transform method. For the first time, an arbitrary heat flux is applied to the heat exchanger wall in contact with the heat transfer fluid, which makes the proposed solution applicable for any wall boundary conditions, including arbitrary heat flux, isothermal, isoflux, adiabatic, as well as mean, linear, and exponential estimation of the heat transfer fluid temperature. Therefore, for the first time, this study will enable the consideration of the variation in the heat transfer fluid temperature to analytically model the heat and mass transfer more accurately and to investigate and establish suitable boundary conditions to design an optimal absorber bed. The present model is validated with experimental data for various absorber configurations, including tube bundles absorbers vertical tubes, and coil absorbers. Also, the effect of the heat transfer fluid temperature variation on the heat and mass transfer in falling film absorbers is investigated.

2. Problem description and assumptions

The coupled heat and mass transfer in a laminar falling film absorption over an inclined plate with an applied arbitrary heat flux is studied, see Fig. 1. It is shown how this solution can be used for other wall conditions – such as adiabatic, isothermal, and variable temperature wall – and applied to other configurations, e.g., vertical and horizontal plates/tubes of the heat exchanger.

A lithium bromide water (LiBr-water) solution is considered as the absorption liquid and introduced at the top of the plate with a uniform

Table 1
Existing analytical solutions for coupled heat and mass transfer in laminar falling film absorption.

Solution Method	Study	Velocity profile	Wall boundary condition
Similarity solution	Nakoryakov and Grigor'eva [23]	Uniform velocity profile	Isothermal
	Nakoryakov and Grigor'eva [24]	Uniform velocity profile	Isothermal
	Nakoryakov and Grigor'eva [25]	Uniform velocity profile	Isothermal
	Grossman [26]	Uniform velocity profile	Isothermal
	Brauner et al. [27]	Uniform velocity profile	Isothermal
	Nakoryakov et al. [18]	Uniform velocity profile	Adiabatic
	Giannetti [28]	Uniform velocity profile	Isothermal
Fourier method/ Expansion series	Nakoryakov and Grigor'eva [29]	Uniform velocity profile	Isothermal
	Grossman [30]	Parabolic velocity profile	Isothermal and adiabatic
	Nakoryakov and Grigor'eva [31]	Uniform velocity profile	Isothermal and adiabatic
	Giannetti et al. [32]	Parabolic velocity profile	Isothermal
	Meyer[33]	Uniform velocity profile	Isothermal and adiabatic
Laplace transform method	Meyer and Ziegler [34]	Uniform velocity profile	Isothermal
	Meyer [35]	Uniform velocity profile	Diabatic wall at a constant heat transfer fluid temperature
	Meyer [36]	Uniform velocity profile	Isothermal and adiabatic
	Mortazavi and Moghaddam [37]	Linear velocity profile	Isothermal
	Ashouri and Bahrami [15]	Power-law velocity profile	Isothermal
	The present study	**Power-law velocity profile**	**An arbitrary heat flux covering all the wall boundary conditions, including isothermal, isoflux, adiabatic, etc. Adding the effect of variation in the heat transfer fluid temperature.**

temperature and concentration and forms a continuous film. The solution is however applicable for other absorption liquids. The film is exposed to water vapor, which is absorbed in the solution-vapor interface and diffuses through the film. As a result of vapor absorption, heat is generated at the interface. The solution is cooled via a heat transfer fluid flowing inside the heat exchanger.

The following summarizes the present model's assumptions [15]:

- The solution film is in laminar regime ($Re = \frac{4\Gamma}{\mu} < 125$ [38]) and the flow is hydrodynamically fully developed. It is justified by considering the Prandtl number for the LiBr-water solution of Pr ~ 20–30 [28] and for LiCl-water Pr ~ 35 [39];
- The thermo-physical properties of the solution are assumed to be constant, i.e., an averaged value for each property may be used over the corresponding temperature and concentration range;
- The absorbent is non-volatile;
- Heat transfer from the film to the vapor phase is neglected since the absorber works at the low pressures (~vacuum condition);
- The mass flow rate variation as a result of the absorbed gas is negligible;
- The drag force at the solution-vapor interface is negligible;
- There is no disturbance or wave at the solution-vapor interface;
- Temperature and concentration distributions are uniform at the entrance region;
- The ratio of film thickness to the radius of the tube should be low (curvature ratio: $CR = \frac{\delta}{R_o} < 0.125$, where δ and R_o are film thickness and tube radius, respectively); and
- Equilibrium exists at the solution-vapor interface and it is approximated with a linear relationship between temperature and concentration at the vapor pressure.

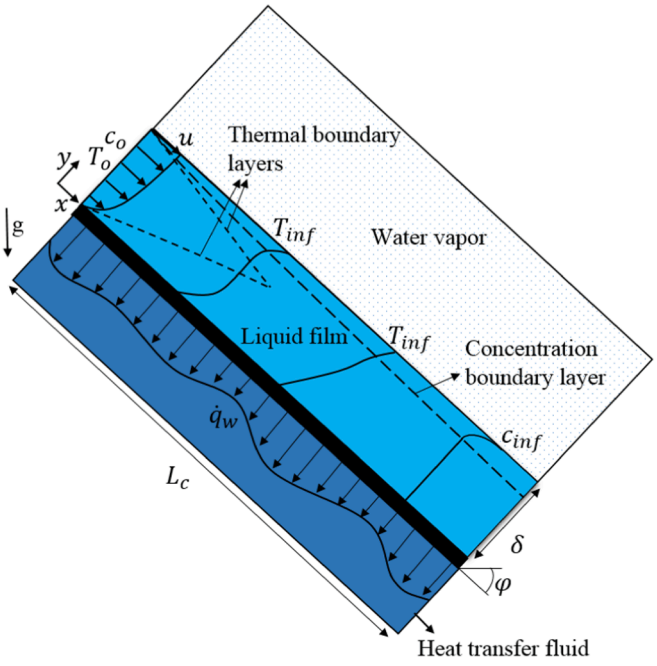

Fig. 1. The schematic diagram of falling film absorption over an inclined plate.

Further details on the justifications for the assumptions can be found in our previous study [15].

3. Model development

The present model is developed based on our previous model [15], where we proposed a new power-law approximation for the velocity profile. The power-law velocity profile has a mean relative difference of 9% with the exact parabolic velocity profile, which is considerably lower than that of the averaged [33] or linear [37] approximations for the velocity profile; thus it is used instead of the exact parabolic velocity profile [15]:

$$u = \frac{3}{2}\bar{u}\sqrt{\eta}\left[\frac{m}{s}\right] \tag{1}$$

$$\bar{u} = \frac{\Gamma}{\rho\delta}\left[\frac{m}{s}\right] \tag{2}$$

$$\delta = \left(\frac{3\Gamma v}{g\rho sin(\varphi)}\right)^{1/3}[m] \tag{3}$$

Table 2
Temperature and concentration profiles for different boundary conditions. Constants can be found in Appendix B.

Parameter	Equation			Eq. No.
Temperature profile in the Laplace space	$\Theta(s,\eta) = c_1\sqrt{s^{0.4}}\eta I_{\frac{2}{5}}\left(\frac{4}{5}(s^{0.4}\eta)^{\frac{5}{4}}\right) + c_2\sqrt{s^{0.4}}\eta K_{\frac{2}{5}}\left(\frac{4}{5}(s^{0.4}\eta)^{\frac{5}{4}}\right)$			(24)
Concentration profile in the Laplace space	$Y(s,\eta) = c_3\sqrt{s^{0.4}}\eta I_{\frac{2}{5}}\left(\frac{4}{5}\sqrt{Le.s}\,(\eta)^{\frac{5}{4}}\right) + c_4\sqrt{s^{0.4}}\eta K_{\frac{2}{5}}\left(\frac{4}{5}\sqrt{Le.s}\,(\eta)^{\frac{5}{4}}\right)$			(25)
Energy equation constants for an arbitrary heat flux	$c_1 = 1.28s^{-0.4}\mathscr{L}\{\dot{Q}_w(\xi)\}(s) + nc_2$		$c_2 = \frac{s^{-1.2} - 1.28\Omega s^{-0.4}\mathscr{L}\{\dot{Q}_w(\xi)\}(s)}{\Psi}$	(26)
Concentration equation constants	$c_3 = nc_4$		$c_4 = \frac{Le}{\Lambda}\frac{c_1\beta_1 + c_2\beta_2}{n\beta_3 + \beta_4}$	(27)
Temperature profile	$\theta(\xi,\eta) = \frac{ln2}{\xi}\sum_{i=1}^{N} V_i\Theta(\frac{ln2}{\xi}i,\eta)$			(28)
Concentration profile	$\gamma(\xi,\eta) = \frac{ln2}{\xi}\sum_{i=1}^{N} V_i Y(\frac{ln2}{\xi}i,\eta)$			(29)
Special cases				
Heat flux as a general expansion series	$c_1 = 1.28\sum_{i=0}^{\infty} a_i\frac{i!}{s^{i+1.4}} + nc_2$		$c_2 = \frac{s^{-1.2} - 1.28\Omega\sum_{i=0}^{\infty} a_i\frac{i!}{s^{i+1.4}}}{\Psi}$	(30)
Variable heat transfer fluid temperature	$c_1 = 1.28s^{-0.4}Bi(\frac{1.28\Omega s^{-0.4}Bi\theta_{HTF}(s) + s^{-1.2}}{1.28\Omega s^{-0.4}Bi + m\Psi} - \theta_{HTF}(s)) + nc_2$			(31)
	$c_2 = \frac{s^{-1.2} - 1.28\Omega s^{-0.4}Bi(\frac{1.28\Omega s^{-0.4}Bi\theta_{HTF}(s) + s^{-1.2}}{1.28\Omega s^{-0.4}Bi + m\Psi} - \theta_{HTF}(s))}{\Psi}$			(32)
Average heat transfer fluid temperature $\theta_{HTF}(s) = \frac{\theta_w}{s}$	Linear heat transfer fluid temperature	$\theta_{HTF}(s) = \frac{\theta_{HTF-out} - \theta_{HTF-in}}{\xi_{@L_C}}\frac{1}{s^2} + \frac{\theta_{HTF-in}}{s}$	Exponential heat transfer fluid temperature	$\theta_{HTF}(s) = \frac{\theta_{HTF-in}}{s - \xi_{@L_C}^{-1}Ln\frac{\theta_{HTF-out}}{\theta_{HTF-in}}}$
Converting the wall heat flux to the heat transfer fluid temperature & vice versa	$\dot{Q}_w(\xi) = \mathscr{L}^{-1}\{Bi\left(\frac{1.28\Omega s^{-0.4}Bi\theta_{HTF}(s) + s^{-1.2}}{1.28\Omega s^{-0.4}Bi + m\Psi} - \theta_{HTF}(s)\right)\}$			(33)
	$\theta_{HTF}(\xi) = \mathscr{L}^{-1}\{\frac{\frac{\mathscr{L}\{\dot{Q}_w(\xi)\}(s)}{Bi} - \frac{s^{-1.2}}{1.28\Omega s^{-0.4}Bi - m\Psi}}{1 - \frac{1.28\Omega s^{-0.4}Bi}{1.28\Omega s^{-0.4}Bi - m\Psi}}\}$			(34)

$$\eta = \frac{y}{\delta} \tag{4}$$

Where δ, η and $\bar{u}$ are the boundary layer thickness, non-dimensional "y", and the average velocity, respectively. Also, ρ and Γ denote the solution density and solution mass flow rate per unit depth, respectively. Advection in the *x*-direction and diffusion in the *y*-direction are the dominant mechanisms for transport in this problem [35]. Therefore, the following governing equations for energy and species concentration can be derived [15]:

$$u\frac{\partial T}{\partial x} = \alpha_s\frac{\partial^2 T}{\partial y^2} \tag{5}$$

$$u\frac{\partial c}{\partial x} = D_s\frac{\partial^2 c}{\partial y^2} \tag{6}$$

where T, α, c and D_s are the solution temperature, thermal diffusivity, absorbate concentration, and mass diffusivity, respectively. Using the equilibrium temperature and concentration, Eqs. (5) and (6) can be non-dimensionalized. The equilibrium temperature "T_{eq}" is the temperature corresponding to the concentration at the entrance and similarly, "c_o" the equilibrium concentration "c_{eq}" is the concentration corresponding to the temperature at the entrance "T_o". Equilibrium temperature and concentration can be calculated via a phase equilibrium equation, see Appendix A. Non-dimensional energy and mass balance equations can be derived as follows [15]:

$$\sqrt{\eta}\,\frac{\partial\theta}{\partial\xi} = \frac{\partial^2\theta}{\partial\eta^2} \tag{7}$$

$$Le\sqrt{\eta}\,\frac{\partial\gamma}{\partial\xi} = \frac{\partial^2\gamma}{\partial\eta^2} \tag{8}$$

$$\theta(\xi,\eta) = \frac{T(\xi,\eta) - T_o}{T_{eq}(c_o,p) - T_o} \tag{9}$$

$$\gamma(\xi,\eta) = \frac{c(\xi,\eta) - c_o}{c_{eq}(T_o,p) - c_o} \tag{10}$$

$$\xi = \frac{x}{\delta^2}\frac{\alpha}{\frac{3}{2}\bar{u}}, \eta = \frac{y}{\delta} \tag{11}$$

Where θ, $\gamma$and ξ represent the non-dimensional temperature, non-dimensional concentration, and the non-dimensional "*x*", respectively. The initial and boundary conditions are as follows:

$$\theta(\xi = 0,\eta) = \frac{T_o - T_o}{T_{eq}(c_o,p) - T_o} = 0 \tag{12}$$

$$\gamma(\xi = 0,\eta) = \frac{c_o - c_0}{c_{eq}(T_o,p) - c_o} = 0 \tag{13}$$

$$\left.\frac{\partial\theta}{\partial\eta}\right|_{\eta=0} = -\frac{\delta}{k_s\left(T_{eq} - T_o\right)}\dot{q}_w(\xi) = \dot{Q}_w(\xi)\ \text{arbitrary heat flux} \tag{14a}$$

$$\left.\frac{\partial\theta}{\partial\eta}\right|_{\eta=0} = \sum_{i=0}^{\infty} a_i\xi^i \text{where } \dot{Q}_w(\xi) \text{ is written as a general expansion series} \tag{14b}$$

$$\left.\frac{\partial\gamma}{\partial\eta}\right|_{\eta=0} = 0 \tag{15}$$

$$\theta(\xi,\eta = 1) + \gamma(\xi,\eta = 1) = 1 \tag{16}$$

Table 3
The operating conditions and configurations of the data from the References [40–43].

Study	Configuration	$L_c(m)$	$\Gamma(kg/ms)$	$P_v(kPa)$	T_o(°C)	T_w(°C)	$c_o(\frac{kg}{kg})$
Islam [40]	Horizontal tube	0.71	0.044	1–3	40	32–37	0.40
Yoon et al. [41]	Helical (coil)	0.25	0.01–0.04	1	45	30	0.40
Sun et al. [42]	Horizontal tube	0.45	0.02	2.1	40–50	32	0.39
Medrano et al. [43]	Vertical tube	1.2	0.084	0.9–1.6	40	30	0.4

Table 4
The properties of the LiBr-water solution [28,37].

Thermophysical property	Value
Dynamic viscosity (Pa.s)	0.005
Density (kg.m^{-3})	1,500
Thermal conductivity (W.m^{-1}.K^{-1})	0.42–0.46
Specific heat capacity (kJ.kg^{-1}.K^{-1})	2
Absorption heat (kJ.kg^{-1})	2,500
Lewis number	80–100

$$\left.\frac{\partial\theta}{\partial\eta}\right|_{\eta=1} = \frac{\Lambda}{Le}\left.\frac{\partial\gamma}{\partial\eta}\right|_{\eta=1} \tag{17}$$

$$\Lambda = \frac{h_{abs}(c_{eq}-c_o)}{c_s(T_{eq}-T_o)} \; and \; Le = \frac{\alpha_s}{D_s} \tag{18}$$

Considering Eq. (18), the Lewis number, Le, for an aqueous LiBr solution is around 100, and the normalized absorption heat, Λ, the range is between 5 and 10. During the absorption process, heat is generated at the solution-membrane interface. The amount of generated heat is the product of the heat of absorption and the absorbed mass. On the other hand, the variation in the solution temperature, as a result of the heat generation, changes water vapor partial pressure at the membrane-solution interface, which leads to a varying concentration and absorption rate. Therefore, heat and mass transfer are highly coupled, via Eqs. (16) and (17).

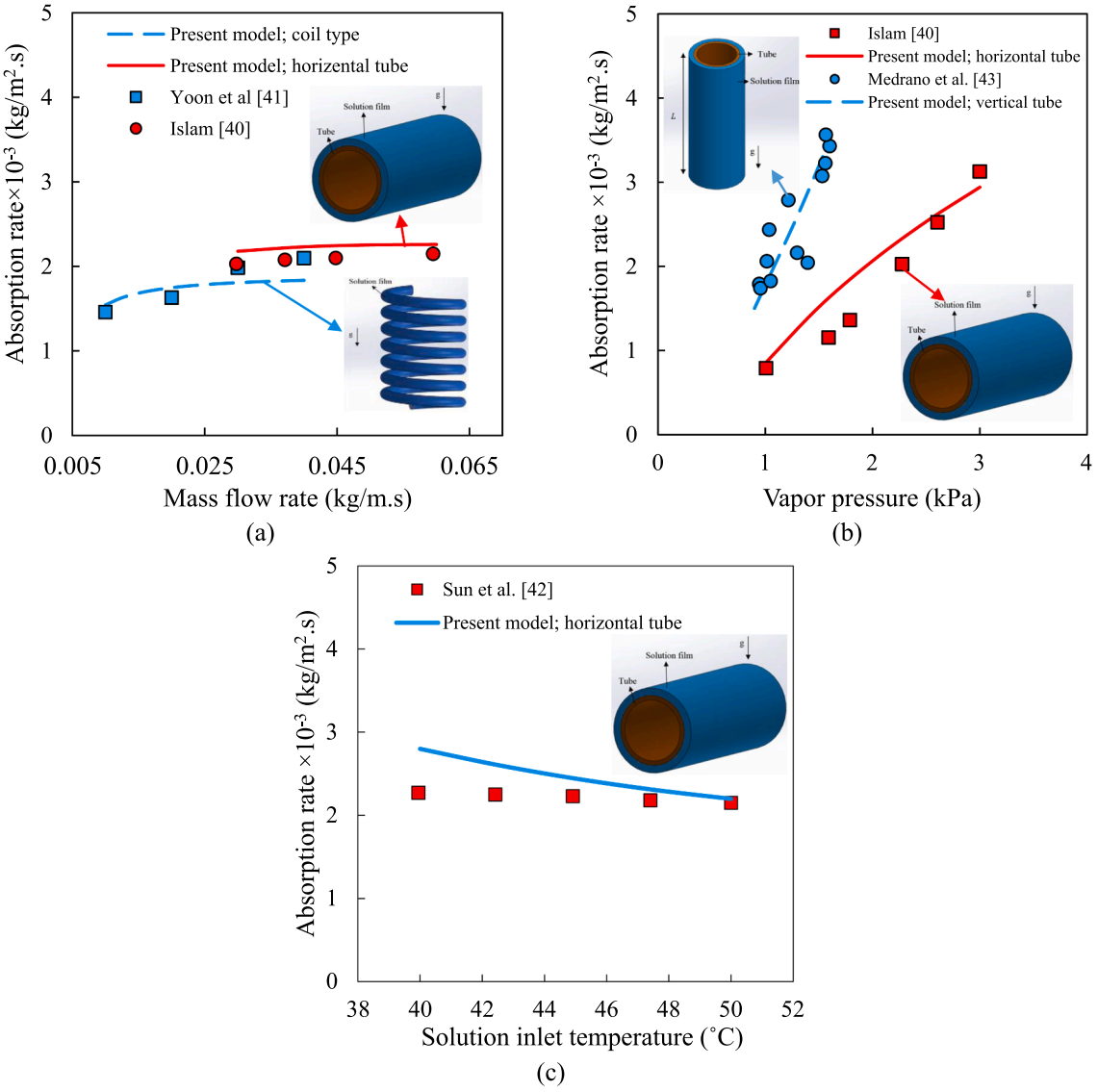

Fig. 2. A comparison between the results obtained by the present model and the experimental results of: (a) Islam [40] and Yoon et al. [41]; (b) Islam [40] and Sun et al. [42]; and (c) Medrano et al. [43].

Table 5
The operating conditions and their non-dimensional form used for investigating the effect of the heat exchanger wall.

Parameter	Value	Parameter	Value
$T_o(°C)$	45	$L_C(m)$	1
$T_{HTF-in}(°C)$	30	θ_{HTF-in}	−1.7
$T_{HTF-ave}(°C)$	36	$\theta_{HTF-out}$	−1
$T_{HTF-out}(°C)$	42	$\theta_{HTF-ave}$	−0.3
$c_o(kg.kg^{-1})$	0.4	Le	100
$p_v(Pa)$	1.74	$Le.\Lambda^{-1}$	14
$\Gamma(kg.m^{-1}s^{-1})$	0.04	$\xi_{@L_C}$	11.5

Considering the heat transfer coefficient of the heat transfer fluid and the heat exchanger wall thermal contact resistance, the thermal boundary condition at the heat exchanger can also be written as follows:

$$\left.\frac{\partial\theta}{\partial\eta}\right|_{\eta=0} = Bi(\theta_w(\xi)-\theta_{HTF}(\xi)) = \dot{Q}_w(\xi) \tag{19}$$

where, θ_{HTF} and the Biot number "Bi" are defined as:

$$\theta_{HTF}(\xi) = \frac{T_{HTF}(\xi)-T_o}{T_{eq}(c_o,p)-T_o} = 0 \tag{20a}$$

$$Bi = \frac{\frac{\delta_s}{k_s}}{\left(\frac{1}{h_{HTF}}+\frac{\delta_w}{k_w}\right)} \tag{20b}$$

where, $T_{HTF}(\xi)$, δ_s, and k_s are the bulk heat transfer fluid temperature varying with non-dimensional "x" or ξ, the solution thickness, and the thermal conductivity, respectively. Also, h_{HTF}, δ_s and k_s are the heat transfer coefficient of the heat transfer fluid, and the heat exchanger wall thickness and thermal conductivity, respectively. For brevity, details of the Laplace transform method are shown in Appendix B. Also, the procedure for generalizing the present analytical model for different absorber configurations is presented in Appendix C. By finding the temperature and concentration distributions from the above-mentioned equations, see Table 2, the heat and mass transfer rates for falling film absorbers can be calculated as follows [15]:

$$\dot{q}(\xi) = \frac{k_s(T_{eq}-T_o)}{\delta}\left.\frac{\partial\theta}{\partial\eta}\right|_{\eta=1}\left[\frac{w}{m^2}\right] \tag{21}$$

$$\dot{m}(\xi) = \frac{\rho_s D_s(c_{eq}-c_o)}{\delta}\left.\frac{\partial\gamma}{\partial\eta}\right|_{\eta=1}\left[\frac{kg}{m^2.s}\right] \tag{22}$$

where, k_s, ρ_s, and D_s are the solution thermal conductivity, density, and mass transfer coefficient, respectively. In Section 4, the mass transfer potential (non-dimensional mass transfer rate) is used for investigating the effect of different wall boundary conditions on the mass transfer rate, and is defined as [34]:

$$\mu_i(\xi) = \left.\frac{\partial\gamma(\xi)}{\partial\eta}\right|_{\eta=1} \tag{23}$$

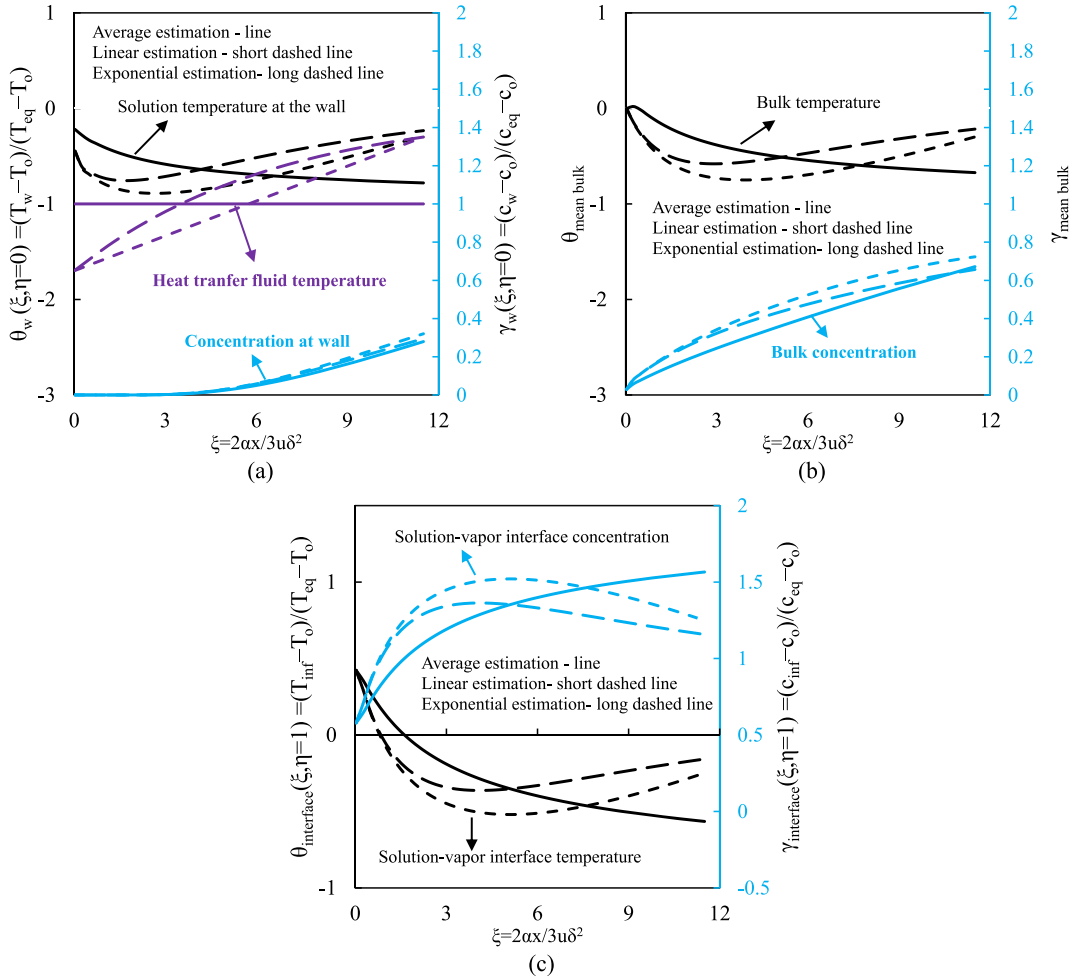

Fig. 3. Non-dimensional temperature and concentration profiles versus non-dimensional "x" or "ξ" at: (a) the wall; (b) mean bulk; and (c) the solution-vapor interface or $\eta = 1$. Black curves show temperature and blues curves represent concentration. Solid line, short dashed, and long dashed lines represent average, linear and exponential heat transfer fluid temperature estimations, respectively.

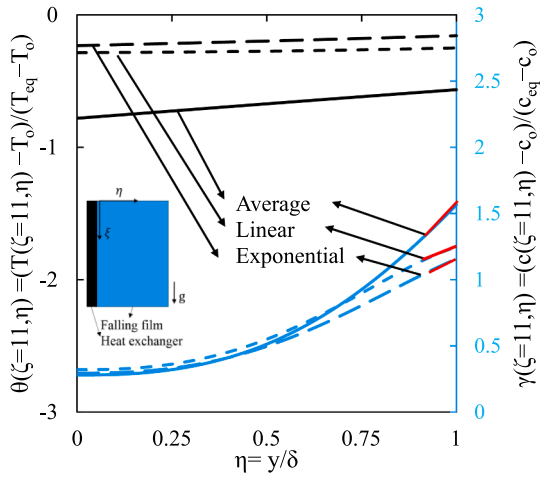

Fig. 4. Non-dimensional temperature and concentration profiles versus non-dimensional "y" or "η" for three different temperature estimations. Black curves show temperature, and blue curves represent concentration. Solid line, short dashed, and long dashed lines represent average, linear, and exponential heat transfer fluid temperature estimations, respectively. (For interpretation of the references to colour in this figure legend, the reader is referred to the web version of this article.)

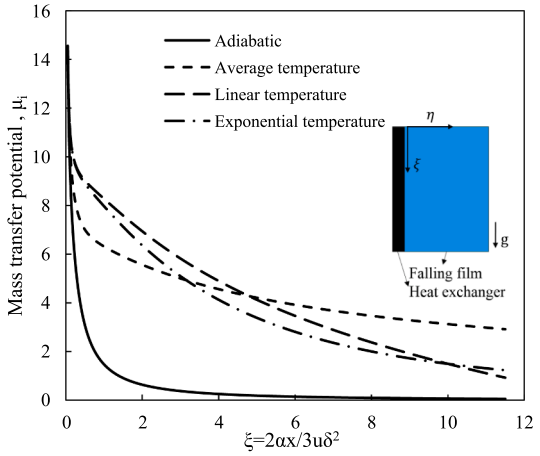

Fig. 5. The mass transfer potential versus non-dimensional "x" or "ξ" at four different wall conditions, including adiabatic and mean, linear and exponential temperature estimations. The mass transfer potential is $\mu_i(\xi) = \left.\frac{\partial\gamma(\xi)}{\partial\eta}\right|_{\eta=1}$.

4. Results and discussion

4.1. Model validation

The present model is validated with experimental data from Refs. [40–43] with their operating conditions and configurations listed in Table 3. The properties of the LiBr-water solution are listed in Table 4.

Fig. 2 shows a comparison between the results obtained by the present model and the experimental data mentioned in Refs. [40–43]. As can be seen, the present model's results follow the trend of the experimental data in Refs. [40–43]. Also, the mean relative differences between the results of the present model and the experimental results of Islam [40], Yoon et al. [41], Sun et al. [42], and Medrano et al. [43] are nearly 13%, 8%, 12%, and 11%, respectively.

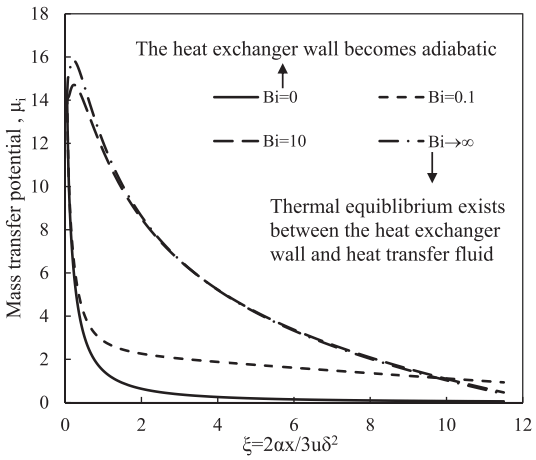

Fig. 6. The mass transfer potential versus non-dimensional "x" or "ξ" at four different Biot numbers for linear heat transfer fluid temperature. The mass transfer potential is $\mu_i(\xi) = \left.\frac{\partial\gamma(\xi)}{\partial\eta}\right|_{\eta=1}$. The Biot number is $\frac{\frac{\delta_s}{k_s}}{\left(\frac{1}{h_{HTF}}+\frac{\delta w}{k_w}\right)}$.

4.2. Effect of the heat exchanger wall boundary condition on the mass transfer rate

This section examines the effect of the heat exchanger wall boundary conditions on the mass transfer rate, temperature, and concentration profiles. As a case study, falling film over a vertical tube with a depth of 1 *m* is considered with an aqueous LiBr as the solution. Table 5 lists the operating conditions and their non-dimensional form used here. The vertical tube length and the operating conditions are selected based on real examples, listed in Table 3, and by considering heat pump applications for which a temperature lift is necessary.

4.2.1. Temperature and concentration profiles considering heat transfer fluid variation

In previous analytical studies, a mean temperature was used for the heat transfer fluid to calculate the coupled heat and mass transfer rates. This assumption is a suitable choice for absorption chillers, where a high mass flow rate for the heat transfer fluid is used to maintain the heat exchanger wall temperature rather constant to enhance the absorption rate. However, for heat pump applications, a temperature lift of 10 – 15C is required. Therefore, assuming a mean temperature for the heat transfer fluid might result in inaccurate results. In this section, we investigate the effect of three heat transfer fluid temperature variations, including the mean, linear, and exponential estimations. The effects of these variations are considered on the temperature and concentration profiles, which determine the heat and mass transfer rates. It should be noted that a Biot number of 1 has been considered here, which means that the heat transfer fluid and the heat exchanger wall have the same temperature, $\theta_w(\xi) \cong \theta_{HFT}(\xi)$. The effect of the Biot number on the mass transfer rate is investigated in the following part.

Fig. 3 shows non-dimensional temperature and concentration profiles versus non-dimensional "*x*" or "ξ" at the heat exchanger wall, mean bulk, and solution-vapor interface, i.e., $\eta = 1$. The following can be observed:

i) By increasing "ξ", the difference between the concentration profiles increases, Fig. 3a. Also, linear and exponential estimations may offer a more realistic result of the absorber bed.
ii) The linear and exponential estimations offer a rather different trend for temperature profiles compared to the mean estimation, Fig. 3b. This difference affects the concentration profiles since the heat and mass transfer are coupled.

iii) At the solution-vapor interface, $\eta = 1$, the difference between the concentration profile predicted by assuming a mean versus linear and exponential estimations becomes more substantial, Fig. 3c.
iv) A non-monotonic behavior can be observed for the solution temperature at the interface, wall, or in the bulk for both linear and exponential estimations. However, a non-monotonic behavior for the solution concentration is only observed at the interface. This behavior cannot be observed in the average concentration of the solution's bulk or at the wall. The reason for this discrepancy lies in the Lewis number of the LiBr-water solution, which is approximately 100. The Lewis number indicates that mass diffusion occurs 100 times slower compared to thermal diffusion. As a result, the bulk concentration does not vary as fast as the concentration at the interface. However, the bulk temperature can still vary in response to changes in the interface temperature and follow the trend of the interface temperature.

Fig. 4 shows non-dimensional temperature and concentration profiles versus non-dimensional "y" or "η" for three different temperature variations. The solution temperature profile for linear and exponential heat transfer fluid temperature profiles are close, while the mean heat transfer fluid temperature profile shows a remarkable difference. The concentration gradient (slope), which determines the mass transfer rate, is demarcated with the red line at the solution-vapor interface or "$\eta = 1$". Linear and exponential estimations are close, yet, the slope for the mean estimation is not the same as linear and exponential estimations.

4.2.2. *Effect of the heat transfer fluid's temperature variation on the absorption rate*

This section examines the effect of variation in the heat transfer fluid's temperature on the absorption rate. Fig. 5 shows the mass transfer potential versus non-dimensional "x" or "ξ" under four wall boundary conditions, including adiabatic and mean, linear, and exponential temperature profile assumptions. The following can be observed:

i) For adiabatic walls, the absorption rate rapidly decreases by increasing "ξ" since there is no heat transfer fluid to maintain the solution temperature.
ii) Linear and exponential estimations show a higher absorption rate at lower "ξ" as compared to mean temperature profile assumption.
iii) Mean temperature profile shows a higher absorption rate at larger "ξ" values than linear and exponential profiles. At the end of the absorber ($\xi = 11.5$ or $x = 1$ m), using mean heat transfer fluid temperature results in up to 3 times higher absorption rate at the outlet region of absorber compared to linear and exponential profile estimations.
iv) Regarding the optimized length of the vertical tube, one can conclude that linear and exponential profile assumptions, which are the case in real heat exchangers, for the heat transfer fluid temperature can lead to a better estimation of the absorber length. In contrast, using an average heat transfer fluid temperature, which is not close to reality based on real heat exchangers, shows a higher mass transfer rate. Therefore, using the linear estimation can lead to overestimating the optimized length of the vertical tube.

4.2.3. *Effect of the Biot number on mass transfer*

Fig. 6 shows the effect of the Biot number on the mass transfer potential for linear heat transfer fluid temperature. The following can be observed:

i) When the Biot number approaches zero, there is no heat transfer between the heat transfer fluid and the heat exchanger wall. Therefore, this case is similar to an adiabatic wall.
ii) When the Biot number approaches infinity, there is a thermal equilibrium between the heat exchanger wall and heat transfer fluid. Thus, the amount of the mass transfer rate is maximum under this condition.

5. Conclusion

This study presented a new analytical solution for non-volatile absorbents to calculate coupled heat and mass transfer in falling film absorbers used in absorption heat pumps and chillers. The Laplace transform method was used to develop the present model. An arbitrary heat flux was applied to the heat exchanger wall in contact with the heat transfer fluid. The present approach led to a generalized model for various heat exchanger wall boundary conditions, including arbitrary heat flux, isothermal, adiabatic, as well as mean, linear, and exponential estimations of the heat transfer fluid temperature. As a result of this generalization, the present analytical model was able to capture the effect of variation in the heat transfer fluid temperature on the heat and mass transfer in falling film absorbers. The present model was validated with experimental data available in the literature with a mean relative difference of 11%. Considering a case study of an absorber with a length of 1 m, it was shown that assuming an average temperature for the heat transfer fluid led to overestimation of the optimal length of the absorber. However, a linear or exponential estimation of heat transfer fluid temperature could lead to more accurate results for designing an optimized absorber bed, particularly for absorption heat pumps for which a temperature lift is a key parameter.

CRediT authorship contribution statement

Mahyar Ashouri: Conceptualization, Investigation, Software, Writing – original draft. **Amin M. Elsafi:** Investigation, Writing – review & editing. **Ilya S. Girnik:** Formal analysis, Investigation, Writing – review & editing. **Majid Bahrami:** Conceptualization, Writing – review & editing, Supervision, Project administration, Funding acquisition.

Declaration of Competing Interest

The authors declare that they have no known competing financial interests or personal relationships that could have appeared to influence the work reported in this paper.

Data availability

No data was used for the research described in the article.

Acknowledgments

This research is supported by funding from the Pacific Institute for Climate Solutions (PICS) Opportunity Grant (No. 36170-50280) and the Natural Sciences and Engineering Research Council of Canada (NSERC) Advancing Climate Change Science in Canada Grant (No. 536076-18). We acknowledge the support of the Natural Sciences and Engineering Research Council of Canada (NSERC) Collaborative Research and Training Experience program, CREATE (No. 554770-2021).

Appendix A. Equation for the phase equilibrium of the LiBr-water solution

The following experimental correlations [34] can be used to calculate the equilibrium temperature and concentration for an LiBr-water solution [34]:

Table A1
Constants for the phase equilibrium Eq. (A.1) [34].

Constant		Value	Constant	Value
a_1	-4.70858×10^{-3}	a_9	1.10477×10^{-4}	
a_2	-1.276757×10^{-3}	a_{10}	4.915398×10^{-3}	
a_3	1.45597×10^{-4}	a_{11}	-7.21234×10^{-8}	
a_4	4.28261×10^{-4}	a_{12}	-5.8121×10^{-4}	
a_5	9.48526×10^{-4}	a_{13}	-2.23738×10^{-5}	
a_6	3.47501×10^{-6}	a_{14}	2.39788×10^{-6}	
a_7	-4.95401×10^{-4}	a_{15}	-6.64049×10^{-6}	
a_8	-5.44472×10^{-5}	a_{16}	4.26683×10^{-6}	

$$-\frac{1}{T}=a_1+a_2(1-c)+a_3\ln\left(\frac{1}{Pa}.p\right)+a_4(1-c)\ln\left(\frac{1}{Pa}.p\right)+a_5(1-c)^2+a_6\ln^2\left(\frac{1}{Pa}.p\right)+a_7(1-c)^2\ln\left(\frac{1}{Pa}.p\right)+a_8(1-c)\ln^2\left(\frac{1}{Pa}.p\right)+a_9(1-c)^2\ln^2\left(\frac{1}{Pa}.p\right)$$
$$+a_{10}(1-c)^3+a_{11}\ln^3\left(\frac{1}{Pa}.p\right)+a_{12}(1-c)^3\ln\left(\frac{1}{Pa}.p\right)+a_{13}(1-c)^3\ln^2\left(\frac{1}{Pa}.p\right)+a_{14}(1-c)\ln^3\left(\frac{1}{Pa}.p\right)+a_{15}(1-c)^2\ln^3\left(\frac{1}{Pa}.p\right)+a_{16}(1-c)^3\ln^3\left(\frac{1}{Pa}.p\right) \tag{A.1}$$

where, T, c, and p, are the temperature, LiBr concentration, and pressure, respectively. Also, a_{1to16} are the corresponding constants, which are represented in Table A.1.

Appendix B. Laplace transform solution

At first, boundary conditions (Eq. (14) to (17)) should be converted by taking the Laplace transform with respect to variable "ξ".

$\left.\frac{\partial\theta}{\partial\eta}\right|_{\eta=0}=\int_0^\infty \dot{Q}_w(\xi)e^{-s\xi}d\xi$ Arbitrary heat flux (B1a).

$\left.\frac{\partial\theta}{\partial\eta}\right|_{\eta=0}=\sum_{i=0}^{\infty}\frac{a_i}{s^{i+1}}$ General expansion series(B1b)

$$\frac{\partial \mathrm{Y}(s,\eta=0)}{\partial\eta}=0 \tag{B2}$$

$$\Theta(s,\eta=1)+\mathrm{Y}(s,\eta=1)=\frac{1}{s} \tag{B3}$$

$$\left.\frac{\partial\Theta(s,\eta=1)}{\partial\eta}\right|_{\eta=1}=\frac{\Lambda}{Le}\left.\frac{\partial \mathrm{Y}(s,\eta=1)}{\partial\eta}\right|_{\eta=1} \tag{B4}$$

Likewise, by taking the Laplace transform from Eqs. (7) and (8), they can be transformed into:

$$s.\sqrt{\eta}\Theta(s,\eta)=\frac{\partial^2\Theta(s,\eta)}{\partial\eta^2} \tag{B5}$$

$$s.Le.\sqrt{\eta}\mathrm{Y}(s,\eta)=\frac{\partial^2\mathrm{Y}(s,\eta)}{\partial\eta^2} \tag{B6}$$

Replacing the variable "η" with $z=s^{0.4}\eta$, Eqs. (B.5) and (B.6) are transformed into:

$$\frac{d^2\Theta}{dz^2}-\sqrt{z}\Theta=0 \tag{B7}$$

$$\frac{d^2\mathrm{Y}}{dz^2}-Le\sqrt{z}\mathrm{Y}=0 \tag{B8}$$

The solution to Eqs. (B.7) and (B.8) can be obtained using the modified Bessel function of the first and second kinds:

$$\Theta(s,\eta)=c_1\sqrt{s^{0.4}\eta}I_{\frac{2}{5}}\left(\frac{4}{5}\left(s^{0.4}\eta\right)^{\frac{5}{4}}\right)+c_2\sqrt{s^{0.4}\eta}K_{\frac{2}{5}}\left(\frac{4}{5}\left(s^{0.4}\eta\right)^{\frac{5}{4}}\right) \tag{B9}$$

$$\mathrm{Y}(s,\eta)=c_3\sqrt{s^{0.4}\eta}\ I_{\frac{2}{5}}\left(\frac{4}{5}\sqrt{Le.s}\,(\eta)^{\frac{5}{4}}\right)+c_4\sqrt{s^{0.4}\eta}\ K_{\frac{2}{5}}\left(\frac{4}{5}\sqrt{Le.s}\,(\eta)^{\frac{5}{4}}\right) \tag{B10}$$

where ,c_1, c_2,c_3, and c_4 are the constants, related to the operating conditions and the properties of a working pair, which can be found in Table 2. The other corresponding parameters are expressed as follows:

$$\Psi=n(k_1+\frac{Le}{\Lambda}\beta_1H)+k_2+\frac{Le}{\Lambda}\beta_2H \tag{B11}$$

$$\Omega=k_1+\frac{Le}{\Lambda}\beta_1H \tag{B12}$$

$$H = \frac{n k_3 + k_4}{n \beta_3 + \beta_4} \tag{B13}$$

$$\beta_1 = p.k_1 + \frac{q}{\sqrt{Le}}(k_5 + \frac{2}{5a} k_1) \tag{B14}$$

$$\beta_2 = p.k_2 + \frac{q}{\sqrt{Le}}(k_6 + \frac{2}{5a} k_2) \tag{B15}$$

$$\beta_3 = p.k_3 + q(k_7 + \frac{2}{5b} k_3) \tag{B16}$$

$$\beta_4 = p.k_4 + q(k_8 + \frac{2}{5b} k_4) \tag{B17}$$

$$k_1 = I_{\frac{2}{5}}(a) \ , \quad k_2 = K_{\frac{2}{5}}(a) \ , \quad k_3 = I_{\frac{2}{5}}(b) \ , \quad k_4 = K_{\frac{2}{5}}(b) \tag{B18}$$

$$k_5 = I_{\frac{7}{5}}(a) \ , \quad k_6 = K_{\frac{7}{5}}(a) \ , \quad k_7 = I_{\frac{7}{5}}(b) \ , \quad k_8 = K_{\frac{7}{5}}(b) \tag{B19}$$

$$p = 0.5\, s^{0.2} \quad , \quad q = \sqrt{Le}\, s^{0.7} \tag{B20}$$

$$a = \frac{4}{5}\sqrt{s} \quad , \quad b = \frac{4}{5}\sqrt{Le.s} \tag{B21}$$

$$m = 0.62497 \ , \quad n = 1.6516 \tag{B22}$$

Finally, by taking the inverse Laplace transform from Eqs. (B.9) and (B.10) using the Stehfest method [44], the temperature and concentration profile can be obtained:

$$\theta(\xi, \eta) = \frac{ln2}{\xi} \sum_{i=1}^{N} V_i \Theta(\frac{ln2}{\xi} i, \eta) \tag{B23}$$

$$\gamma(\xi, \eta) = \frac{ln2}{\xi} \sum_{i=1}^{N} V_i \Upsilon(\frac{ln2}{\xi} i, \eta) \tag{B24}$$

where, V_i is defined as follows:

$$V_i = (-1)^{\frac{N}{2}+j} \sum_{k=\lfloor \frac{i+1}{2} \rfloor}^{\min(i,\frac{N}{2})} \frac{k^{\frac{N}{2}}(2k)!}{(\frac{N}{2}-k)!k!(k-1)!(j-k)!(2k-j)!} \tag{B25}$$

Appendix C. Solution generalization to different configurations

To generalize the analytical solution for calculating the heat and mass transfer over an inclined plate to other geometries, the average film thickness should be calculated by integrating Eq. (3) from 0 to π. For instance, to calculate the heat and mass transfer over a horizontal tube with a circular cross section, as shown in Fig. C1, the following average film thickness is obtained:

$$\delta_{ave} = \frac{1}{\pi} \int_0^{\pi} (\frac{3\Gamma v}{g\rho sin(\varphi)})^{1/3} d\varphi = 1.33\delta_{verticalplate} \tag{c1}$$

The average film thickness is then used to calculate the average velocity and non-dimensional tangential distance ξ:

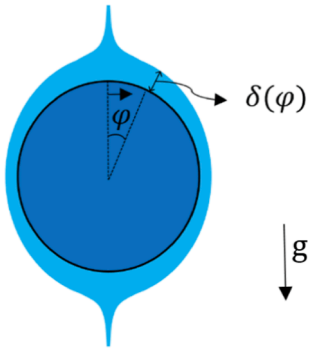

Fig. C1. A schematic diagram of the solution film over a horizontal tube.

$$\bar{u} = \frac{\Gamma}{\rho_s \delta_{ave}} \tag{c2}$$

$$\xi = \frac{2}{3}\frac{x}{\delta_{ave}^2}\frac{\alpha}{\bar{u}} = \frac{2}{3}\frac{x}{\delta_{ave}}\frac{\alpha\rho_s}{\Gamma} \tag{c3}$$

References

[1] A. Salari, M. Ashouri, A. Hakkaki-Fard, On the performance of inclined rooftop solar chimney integrated with photovoltaic module and phase change material: a numerical study, Sol. Energy. 211 (2020) 1159–1169.
[2] M. Ashouri, A. Hakkaki-Fard, Improving the performance of the finned absorber inclined rooftop solar chimney combined with composite PCM and PV module, Sol. Energy 228 (2021) 562–574, https://doi.org/10.1016/J.SOLENER.2021.09.088.
[3] Natural Resources Canada, Renewable energy facts, (n.d.).
[4] I.E.A.D. of S.E. Policy,, Transition to sustainable buildings: strategies and opportunities to 2050, Organization for Economic, 2013.
[5] B. Cárdenas, L. Swinfen-Styles, J. Rouse, A. Hoskin, W. Xu, S.D. Garvey, Energy storage capacity vs. renewable penetration: a study for the UK, Renew. Energy. 171 (2021) 849–867.
[6] H. Bahrehmand, M. Bahrami, Optimized sorber bed heat and mass exchangers for sorption cooling systems, Appl. Therm. Eng. 185 (2021), 116348, https://doi.org/10.1016/J.APPLTHERMALENG.2020.116348.
[7] Roadmap 2030 | CleanBC, (n.d.). https://cleanbc.gov.bc.ca/ (accessed August 27, 2022).
[8] The Paris Agreement | UNFCCC, (n.d.). https://unfccc.int/process-and-meetings/the-paris-agreement/the-paris-agreement (accessed August 27, 2022).
[9] S.F. Zheng, U. Gross, X.D. Wang, Dropwise condensation: From fundamentals of wetting, nucleation, and droplet mobility to performance improvement by advanced functional surfaces, Adv. Colloid Interface Sci. 295 (2021), https://doi.org/10.1016/j.cis.2021.102503.
[10] M. Amani, S. Foroushani, M. Sultan, M. Bahrami, Comprehensive review on dehumidification strategies for agricultural greenhouse applications, Appl. Therm. Eng. 181 (2020), 115979, https://doi.org/10.1016/j.applthermaleng.2020.115979.
[11] X. Zhang, M. Li, W. Shi, B. Wang, X. Li, Experimental investigation on charging and discharging performance of absorption thermal energy storage system, Energy Convers. Manag. 85 (2014) 425–434.
[12] M. Ashouri, M. Bahrami, Analytical solution for coupled heat and mass transfer in membrane-based absorbers, Int. J. Heat Mass Transf. 192 (2022), 122892.
[13] J. Yoo, S. Han, Y. Nam, S. Jeong, Effect of shot-peening on the passive film formation and corrosion of carbon steel in LiBr aqueous solution, J. Mech. Sci. Technol. 34 (10) (2020) 4037–4041.
[14] C. Zhai, W. Wu, Heat and mass transfer performance comparison of various absorbers/desorbers towards compact and efficient absorption heat pumps, Int. J. Refrig. 127 (2021) 203–220.
[15] M. Ashouri, M. Bahrami, Heat and mass transfer in laminar falling film absorption: a compact analytical model, Int. J. Heat Mass Transf. 188 (2022), 122598, https://doi.org/10.1016/J.IJHEATMASSTRANSFER.2022.122598.
[16] X. Liao, R. Radermacher, Absorption chiller crystallization control strategies for integrated cooling heating and power systems, Int. J. Refrig. 30 (2007) 904–911, https://doi.org/10.1016/j.ijrefrig.2006.10.009.
[17] M. Perier-Muzet, B. Stutz, Numerical study of the effectiveness of a vertical falling plate film absorber for an absorption chiller, Int. J. Refrig. 127 (2021) 221–229.
[18] V.E. Nakoryakov, N.I. Grigoryeva, M.V. Bartashevich, Heat and mass transfer in the entrance region of the falling film: absorption, desorption, condensation and evaporation, Int. J. Heat Mass Transf. 54 (2011) 4485–4490, https://doi.org/10.1016/j.ijheatmasstransfer.2011.06.032.
[19] A.M. Elsafi, M. Ashouri, M. Bahrami, A similarity solution for laminar forced convection heat transfer from solid spheres, Int. J. Heat Mass Transf. 196 (2022), 123310.
[20] N. Giannetti, A. Rocchetti, S. Yamaguchi, K. Saito, Analytical solution of film mass-transfer on a partially wetted absorber tube, Int. J. Therm. Sci. 118 (2017) 176–186.
[21] Y. Wu, Simultaneous heat and mass transfer in laminar falling film on the outside of a circular tube, Int. J. Heat Mass Transf. 93 (2016) 1089–1099.
[22] M. Ashouri, M. Bahrami, On the absorption rate of membrane-based adiabatic sorber beds: an analytical approach, Int. J. Heat Mass Transf. 209 (2023), 124105.
[23] V.E. Nakoryakov, N.I. Grigor'eva, Combined heat and mass transfer during absorption in drops and films, J. Eng. Phys. 32 (1977) 243–247, https://doi.org/10.1007/BF00865776.
[24] V.E. Nakoryakov, N.I. Grigor'Eva, Calculation of heat and mass transfer in nonisothermal absorption on the initial portion of a downflowing film, Theor. Found. Chem. Eng. 14 (1980) 483–488.
[25] V.E. Nakoryakov, N.I. Grigoreva, Heat and mass transfer in film absorption with varying liquid-phase volume, Theor. Found. Chem. Eng. 29 (1995).
[26] G. Grossman, Analysis of interdiffusion in film absorption, Int. J. Heat Mass Transf. 30 (1987) 205–208, https://doi.org/10.1016/0017-9310(87)90075-5.
[27] N. Brauner, D.M. Maron, H. Meyerson, Coupled heat condensation and mass absorption with comparable concentrations of absorbate and absorbent, Int. J. Heat Mass Transf. 32 (10) (1989) 1897–1906.
[28] N. Giannetti, S. Yamaguchi, K. Saito, Simplified expressions of the transfer coefficients on a partially wet absorber tube, Int. J. Refrig. 105 (2019) 135–147, https://doi.org/10.1016/j.ijrefrig.2018.07.007.
[29] N.I. Grigor'eva, V.E. Nakoryakov, Exact solution of combined heat-and mass-transfer problem during film absorption, J. Eng. Phys. 33 (5) (1977) 1349–1353.
[30] G. Grossman, Simultaneous heat and mass transfer in film absorption under laminar flow, Int. J. Heat Mass Transf. 26 (1983) 357–371, https://doi.org/10.1016/0017-9310(83)90040-6.
[31] V.E. Nakoryakov, N.I. Grigor'eva, L.V. Potaturkina, Analysis of exact solutions to heat-and mass-transfer problems for absorption with films or streams, Theor. Found. Chem. Eng. 31 (1997) 119–126.
[32] N. Giannetti, A. Rocchetti, S. Yamaguchi, K. Saito, Heat and mass transfer coefficients of falling-film absorption on a partially wetted horizontal tube, Int. J. Therm. Sci. 126 (2018) 56–66, https://doi.org/10.1016/j.ijthermalsci.2017.12.020.
[33] T. Meyer, Improvement of the exact analytical solutions for combined heat and mass transfer problems obtained with the Fourier method, Int. J. Refrig. 43 (2014) 133–142, https://doi.org/10.1016/J.IJREFRIG.2014.04.005.
[34] T. Meyer, F. Ziegler, Analytical solution for combined heat and mass transfer in laminar falling film absorption using first type boundary conditions at the interface, Int. J. Heat Mass Transf. 73 (2014) 141–151.
[35] T. Meyer, Analytical solution for combined heat and mass transfer in laminar falling film absorption with uniform film velocity-diabatic wall boundary, Int. J. Heat Mass Transf. 80 (2015) 802–811.
[36] T. Meyer, Analytical solution for combined heat and mass transfer in laminar falling film absorption with uniform film velocity–Isothermal and adiabatic wall, Int. J. Refrig. 48 (2014) 74–86.
[37] M. Mortazavi, S. Moghaddam, Laplace transform solution of conjugate heat and mass transfer in falling film absorption process, Int. J. Refrig. 66 (2016) 93–104.
[38] M.M.K. Mikhaeel, A.M. Jacobi, Using thermodynamic availability to predict the transitional film reynolds number between the jet and sheet modes in falling liquid between horizontal tubes, Int. J. Heat Mass Transf. 161 (2020), 120246.
[39] M.R. Conde, Properties of aqueous solutions of lithium and calcium chlorides: formulations for use in air conditioning equipment design, Int. J. Therm. Sci. 43 (2004) 367–382.
[40] M.R. Islam, Absorption process of a falling film on a tubular absorber: an experimental and numerical study, Appl. Therm. Eng. 28 (11-12) (2008) 1386–1394.
[41] J.-I. Yoon, O.-K. Kwon, P.K. Bansal, C.-G. Moon, H.-S. Lee, Heat and mass transfer characteristics of a small helical absorber, Appl. Therm. Eng. 26 (2-3) (2006) 186–192.
[42] J. Sun, L. Fu, S. Zhang, W. Hou, A mathematical model with experiments of single effect absorption heat pump using LiBr–H2O, Appl. Therm. Eng. 30 (17-18) (2010) 2753–2762.
[43] M. Medrano, M. Bourouis, A. Coronas, Absorption of water vapour in the falling film of water–lithium bromide inside a vertical tube at air-cooling thermal conditions, Int. J. Therm. Sci. 41 (9) (2002) 891–898.
[44] H. Stehfest, Algorithm 368: numerical inversion of Laplace transforms [D5], Commun. ACM. 13 (1970) 47–49.